Twin Matter Waves for Interferometry Beyond the Classical Limit

B. Lücke, *et al.*

Science **334**, 773 (2011);
DOI: 10.1126/science.1208798

Twin Matter Waves for Interferometry Beyond the Classical Limit

B. Lücke,[1]* M. Scherer,[1]* J. Kruse,[1] L. Pezzé,[2] F. Deuretzbacher,[3] P. Hyllus,[4] O. Topic,[1] J. Peise,[1] W. Ertmer,[1] J. Arlt,[5] L. Santos,[3] A. Smerzi,[2] C. Klempt[1]†

Interferometers with atomic ensembles are an integral part of modern precision metrology. However, these interferometers are fundamentally restricted by the shot noise limit, which can only be overcome by creating quantum entanglement among the atoms. We used spin dynamics in Bose-Einstein condensates to create large ensembles of up to 10^4 pair-correlated atoms with an interferometric sensitivity $-1.61^{+0.98}_{-1.1}$ decibels beyond the shot noise limit. Our proof-of-principle results point the way toward a new generation of atom interferometers.

Atom interferometers exploit the wave nature of matter, providing a unique tool for modern precision metrology (*1*, *2*); most prominently, they have been used to define the second (*3*, *4*). However, interferometers with uncorrelated atoms are fundamentally limited by shot noise (*5*), a remnant of the atoms' particle nature. This limit can be overcome by creating entanglement between the atoms (*6*). Recently, this has been demonstrated for spin-squeezed samples (*7*–*12*). The ultimate Heisenberg limit, where the sensitivity scales linearly with the number of atoms, has been predicted for highly entangled states, such as NOON (*13*) and twin Fock states (*14*). However, they have only been created with up to five photons (*15*–*19*) or six ions (*20*, *21*), but not with neutral atoms. Spin dynamics has been proposed as a possible mechanism to turn a large fraction of an atomic Bose-Einstein condensate into a mixture of twin Fock states (*22*, *23*).

In an interferometric measurement, an ensemble of N_{tot} particles undergoes a sequence that distributes the particles over two independent modes +1 and −1. The possible many-particle states are best described by the collective spin $J = N_{\mathrm{tot}}/2$ and the population imbalance $J_z = (N_{+1} - N_{-1})/2$, where $N_{\pm 1}$ are the mode populations in the ±1 mode. The collective spin can be visualized on the generalized Bloch sphere, where the z coordinate represents the population imbalance J_z and the azimuthal angle represents the relative phase between the two modes. The spin uncertainties can be visualized as the extent of the state on the sphere. For instance, unentangled states spin polarized along the x direction have symmetric uncertainties in relative phase and number, restricted by the uncertainty relation (Fig. 1 A). A typical interferometer sequence results in a rotation of the input state on the Bloch sphere by an angle θ, which depends on the observable of interest. The rotation angle is mapped onto the population imbalance that is finally measured. For unentangled input states, the measurement of the rotation angle is limited by shot noise $\Delta\theta = \sigma(J_z)/(\sqrt{n}|d\langle J_z\rangle/d\theta|) \geq 1/\sqrt{nN_{\mathrm{tot}}}$, where $\sigma(J_z)$ is the standard deviation of the population imbalance and n is the number of independent interferometric measurements.

A measurement beyond the shot noise limit involves a reduction of the output uncertainty at the expense of an increased uncertainty of the conjugate observable, as has been realized by spin squeezing (*8*, *9*, *11*, *12*). An extreme case is provided by the twin Fock state, where the number of particles in the two modes is exactly equal. Because the relative number uncertainty vanishes, the relative phase is completely undetermined. The twin Fock state is hence represented by an arbitrarily thin line around the equator of the Bloch sphere (Fig. 1 B). A rotation of this state maps the quantity of interest not on the expectation value of the output $\langle J_z\rangle$ but rather on its fluctuations $\langle J_z^2\rangle$ (*24*). The resulting sensitivity overcomes the shot noise limit, and is only bound by the Heisenberg limit $\Delta\theta \propto 1/N_{\mathrm{tot}}$. Such an interferometer with twin Fock input states has been created for very small samples, including single (*15*) and double (*16*, *25*) pairs of photons, and a single pair of $^9Be^+$ ions (*20*).

We use spin dynamics in Bose-Einstein condensates for the creation of up to 10^4 paired neutral atoms in two different spin states. To generate these nonclassical states of matter, we start with a Bose-Einstein condensate with horizontal spin orientation (Zeeman substate $m_F = 0$). In these ensembles, collisions may produce correlated pairs of atoms with spins up and down ($m_F = \pm 1$) (*22*, *23*). These collisions are bosonically enhanced if the output modes are occupied. Therefore, they act as a parametric amplifier for a finite initial population in $m_F = \pm 1$ or for pure vacuum fluctuations (*26*). During the parametric amplification of vacuum (*27*), the total number of atoms produced in $m_F = \pm 1$ and its fluctuations increase exponentially with time. The conjugate variable of the total number is the sum of the two atomic phases, whose fluctuations are exponentially damped (*28*). Furthermore, the number difference between $m_F = \pm 1$ atoms is zero (without fluctuations), and hence the corresponding conjugate variable, the relative phase, is fully undetermined. The underlying physics closely resembles that of optical parametric down-conversion in nonlinear crystals, currently the most important technique to generate nonclassical states of light.

The experiments are started by creating a ^{87}Rb condensate of 2.8×10^4 atoms in the hyperfine state $F = 2$, $m_F = 0$ in an optical dipole trap (Fig. 2 A). We initiate the spin dynamics at a magnetic field of 1.23 G, where an excited spatial mode is populated and vacuum fluctuations are amplified (*29*). The states $F = 2$, $m_F = \pm 1$ are populated by spin dynamics for an optimal duration of 15 ms (*29*). Subsequently, the dipole trap is switched off and all three spin components are recorded by absorption imaging (Fig. 2, B and C).

In a sequence of 200 realizations, the total number of atoms N_{tot} in $m_F = \pm 1$ fluctuates strongly, but we observe ultralow fluctuations of the

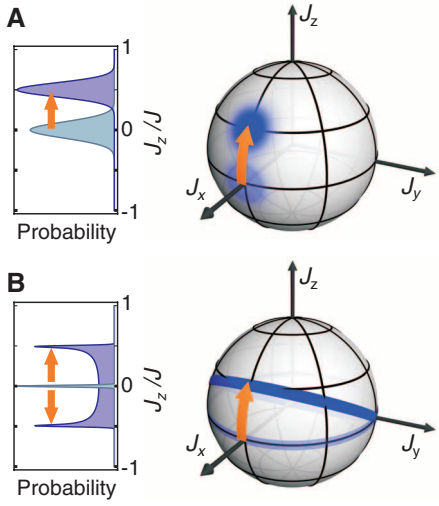

Fig. 1. Interferometric sensitivity of an unentangled and a twin Fock state. The blue shaded regions represent the uncertainty of the corresponding states. (**A**) Geometric representation of the sensitivity of an unentangled input state. A rotation on the Bloch sphere is detected by measuring the expectation value of J_z. (**B**) Geometric representation of the sensitivity of a twin Fock input state. Initially, the ±1 states are equally populated $\langle J_z\rangle = 0$ and the relative phase is undefined; the state is represented by a ring around the equator. After a rotation, the ±1 states are still populated equally $\langle J_z\rangle = 0$, but the tilt of the ring indicates fluctuations $\sigma(J_z)$ increasing with the rotation angle.

[1]Institut für Quantenoptik, Leibniz Universität Hannover, 30167 Hannover, Germany. [2]Istituto Nazionale di Ottica (INO), Consiglio Nazionale delle Ricerche (CNR), and European Laboratory for Non-Linear Spectroscopy (LENS), 50125 Firenze, Italy. [3]Institut für Theoretische Physik, Leibniz Universität Hannover, 30167 Hannover, Germany. [4]Department of Theoretical Physics, The University of the Basque Country, 48080 Bilbao, Spain. [5]Center for Quantum Optics (QUANTOP), Institut for Fysik og Astronomi, Aarhus Universitet, 8000 Århus C, Denmark.

*These authors contributed equally to this work.
†To whom correspondence should be addressed. E-mail: klempt@iqo.uni-hannover.de

population imbalance, represented by the standard deviation $\sigma(J_z)$ (Fig. 2D). This standard deviation shows almost no dependence on the total number of atoms and is compatible with a number-independent detection noise of $\sigma_{dn}(J_z) = 20$ atoms. The detection noise of 20(1) atoms has been measured independently and is dominated by the shot noise of the electrons in the charge-coupled device camera pixels corresponding to a calculated minimum noise contribution of 17 atoms. At a total number of 7800 ±1000 atoms, the variance of J_z including all noise sources is measured to be $-6.91^{+0.89}_{-0.99}$ dB below the shot noise limit. Although we expect atom loss (mainly to other Zeeman and hyperfine states) to prevent the production of perfect twin Fock states, those imperfections are much smaller than the detection noise and thus negligible in our current experimental scheme. The produced pair-correlated state hence constitutes a promising candidate to obtain sub–shot-noise sensitivity in an interferometer.

A test of this sensitivity requires the implementation of an internal-state beam splitter. To drive the transition connecting the $F = 2$, $m_F = \pm 1$ states, we use three resonant microwave pulses (Fig. 3A). On the Bloch sphere, the full sequence represents a rotation around the x axis by an angle $\theta = \tau\Omega_R$, where τ represents the duration of the coupling pulse and Ω_R is the Rabi frequency. Figure 3C shows the standard deviation of the normalized population imbalance $\sigma(J_z/J)$ as a function of the rotation angle θ. It illustrates that the phase to be measured in the interferometer is mapped onto the fluctuations of the output instead of the expectation value. As the picture of

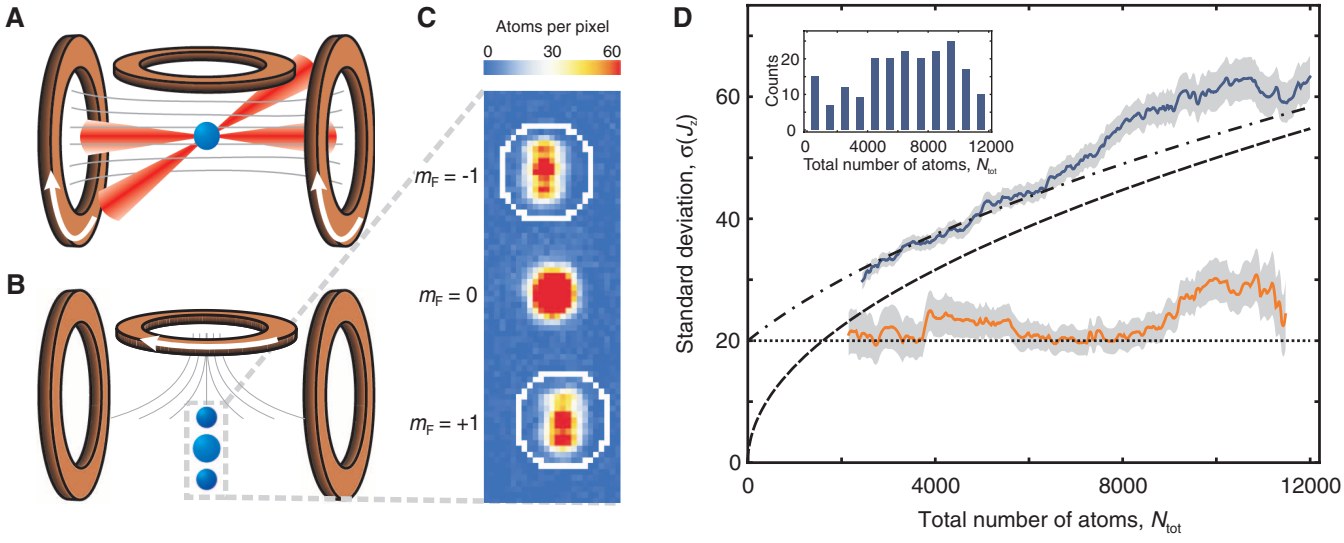

Fig. 2. Preparation and analysis of the input state. (**A**) At a homogeneous magnetic field, a Bose-Einstein condensate in a crossed-beam optical dipole trap generates atoms in the states $m_F = \pm 1$. (**B**) Afterwards, the trap is switched off and the three Zeeman sublevels are split by a strong magnetic field gradient. (**C**) Finally, the three clouds are detected by absorption imaging, and the number of atoms is counted within circular masks (white line). (**D**) Distribution of the relative number of atoms in $m_F = \pm 1$. The measured standard deviation of the population imbalance $\sigma(J_z)$ (orange line) is well below the shot noise limit (dashed line) and mainly limited by the detection noise (dotted line). The experimental result for unentangled atoms (blue line) corresponds to the combination of shot noise and detection noise (dash-dotted line). The shaded area indicates the error of the standard deviation. Inset: Distribution of the total number of atoms. The total number of atoms N_{tot} fluctuates strongly as a result of the amplification of vacuum fluctuations.

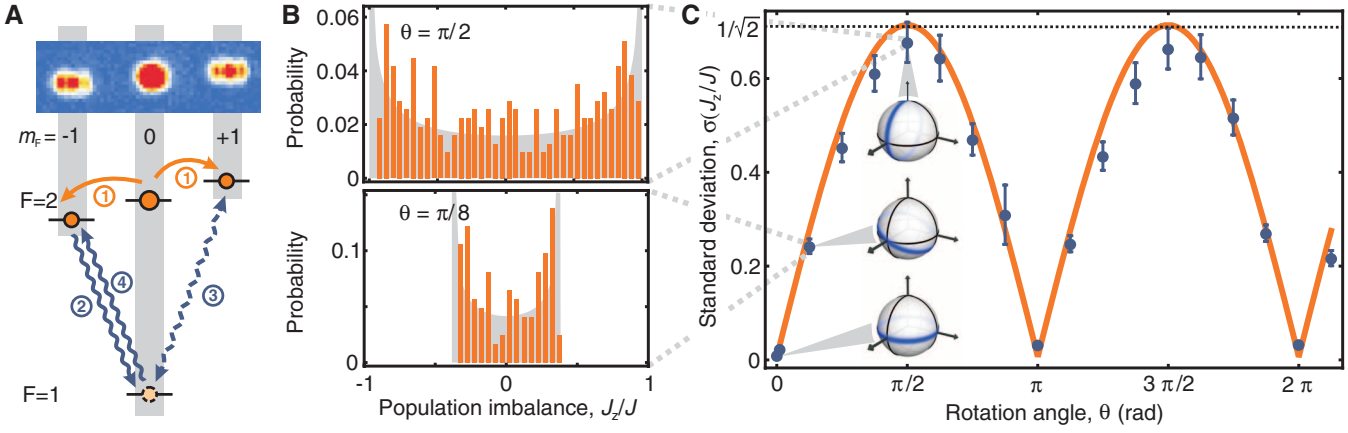

Fig. 3. Internal-state beam splitter for nonclassical matter waves. (**A**) Schematic of the beam splitter sequence. (1) Spin dynamics initially populates the states $|F = 2, m_F = \pm 1\rangle$. (2) To couple these states, the atoms in $|2,-1\rangle$ are transferred to $|1,0\rangle$ by a microwave pulse. (3) Next, a pulse of variable duration τ couples the states $|2,+1\rangle$ and $|1,0\rangle$. (4) Finally, atoms in $|1,0\rangle$ are transferred to the state $|2,-1\rangle$ to enable their independent detection. (**B**) Distribution of the normalized population imbalance for two coupling pulse durations. The strongest fluctuations are obtained for a coupling pulse duration corresponding to a symmetric $\theta = \pi/2$ beam splitter. The shaded area corresponds to the ideal result. (**C**) Fluctuation of the normalized population imbalance. As expected from the representation on the Bloch sphere, the standard deviation $\sigma(J_z/J)$ oscillates as $|\sin\theta|/\sqrt{2}$ as a function of the rotation angle θ. All quantities were obtained for N_{tot} between 3000 and 8000 atoms.

the rotating ring on the Bloch sphere suggests, the standard deviation oscillates approximately as $\sigma(J_z/J) = \alpha|\sin\theta|$, where α characterizes the interferometric contrast. Similar to optical interferometers, the contrast relies heavily on an identical spatial mode of the two input states. Although single-mode operation can be guaranteed for small samples in tight traps, the creation of large samples demands more careful consideration. Generally, spin dynamics populates various spatial modes (*30*), creating multiple twin Fock states without a common phase relation. After the beam splitter, a multimode state yields a number distribution that is a convolution of many single-mode distributions, resulting in a severe reduction of the contrast. We have optimized the configuration for single-mode operation (*29*) and reach a contrast $\alpha = 0.67(0.04)$, close to the ideal value of $\alpha = 1/\sqrt{2} \approx 0.71$.

The symmetric beam splitter obtained for $\theta = \pi/2$ is of special interest. It turns the ring on the Bloch sphere onto the *xz* plane, leading to a maximal uncertainty of the population imbalance and consequently a minimal relative phase uncertainty. It is therefore an optimal state to detect the phase evolution during a Ramsey sequence. Figure 3B shows the distribution of the normalized population imbalance. For $\theta = \pi/2$, it assumes a characteristic shape (*31*) that reflects a high probability of detecting most of the atoms in one of the output ports. Ideally, either all even or all odd numbers should appear in the distribution of the population imbalance J_z, but this parity effect is not accessible within our experiments owing to detection noise and particle losses.

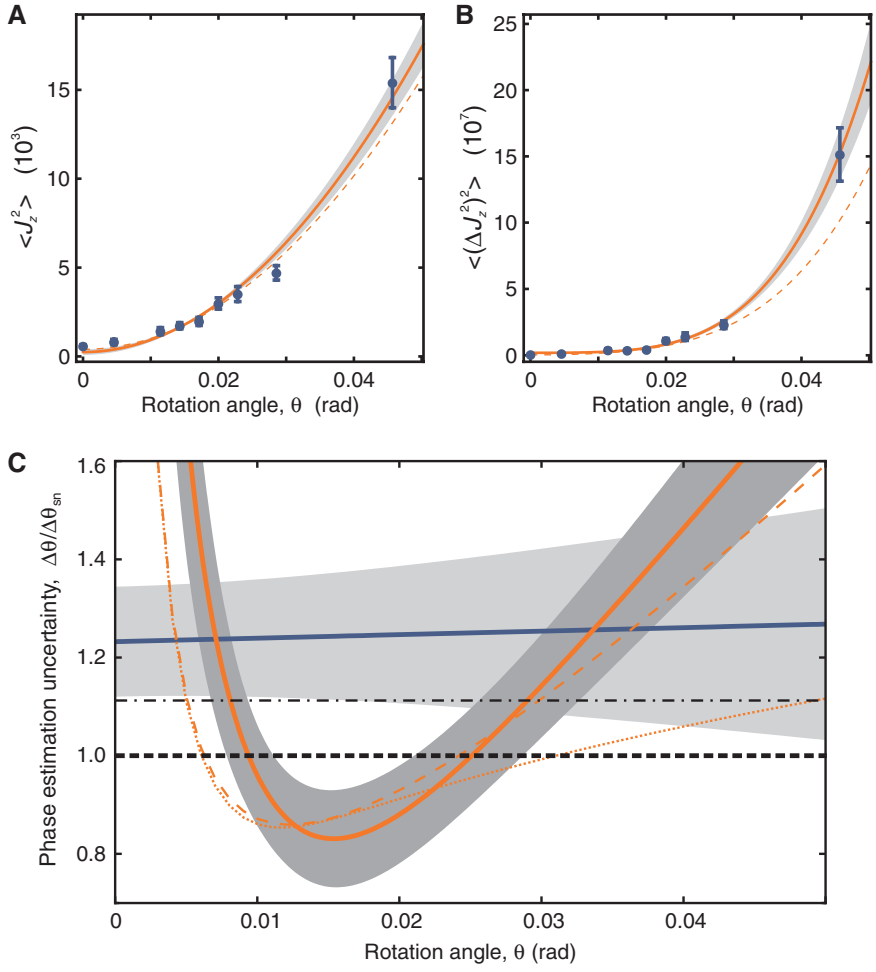

Fig. 4. Phase sensitivity of the pair-correlated state. (**A**) Variance of the population imbalance $\langle \sigma(J_z)^2 \rangle = \langle J_z^2 \rangle$ for a total number N_{tot} between 6400 and 7600 atoms as a function of the rotation angle θ. The orange line is a quadratic fit to the data (*29*), and the shaded area indicates the uncertainty of the fit. Orange dashed line: the theoretical prediction for a detection noise of 20 atoms. (**B**) Same for the fourth moment of the population imbalance $\langle (\Delta J_z^2)^2 \rangle = \langle J_z^4 \rangle - \langle J_z^2 \rangle^2$. (**C**) Sensitivity of the nonclassical state. The phase estimation uncertainty $\Delta\theta$ with respect to shot noise $\Delta\theta_{sn} = 1/\sqrt{n\langle N_{tot} \rangle}$ (solid orange line) is obtained from the fits in (A) and (B) and compared to the expected sensitivity (dashed orange line). At $\theta \approx 0.015$ rad, the phase sensitivity lies $-1.61^{+0.98}_{-1.1}$ dB below the shot noise limit (black dashed line). For a range of values of θ, it is very close to the best achievable value given by the Cramer-Rao lower bound (dotted orange line) (*29*). The experimentally measured sensitivity of an unentangled state (solid blue line) is measured by applying a $\pi/2$ beam splitter to a spin-polarized condensate. The technical noise of the beam splitter causes the measured sensitivity to lie slightly above the combination of shot noise and detection noise (black dash-dotted line).

Based on the beam splitter, we demonstrate that the experimentally created state is entangled and useful for sub–shot-noise interferometry. The phase estimation uncertainty $\Delta\theta$ is inferred from the state's sensitivity to small rotations around an arbitrary axis in the *xy* plane. It is deduced from error propagation according to $\Delta\theta = \Delta J_z^2 / (\sqrt{n} |d\langle J_z^2 \rangle / d\theta|)$ for *n* independent repetitions of the interferometric measurement. In our case, we only rotate the state around the *x* axis, which is less susceptible to technical noise than a Ramsey sequence because of its short duration. The expectation values $\langle J_z^2 \rangle$ and $\langle (\Delta J_z^2)^2 \rangle = \langle J_z^4 \rangle - \langle J_z^2 \rangle^2$ are shown in Fig. 4, A and B, for small rotation angles θ. The result agrees well with the ideal case, including a finite detection noise (*29*). The slight deviation for larger angles indicates additional technical noise, such as magnetic field noise or microwave intensity noise. Polynomial fits (*29*) allow for a precise estimate of the sensitivity (Fig. 4C) according to the error propagation. At the optimal point ($\theta = 0.015$), we reach a measurement uncertainty $\Delta\theta/\Delta\theta_{sn} = 0.83(0.1)$, which is $-1.61^{+0.98}_{-1.1}$ dB below the shot noise limit $\Delta\theta_{sn} = 1/\sqrt{n\langle N_{tot} \rangle}$. This result is also $-2.5^{+0.98}_{-1.1}$ dB below the optimal classical result achievable with our apparatus when both shot noise and detection noise are considered.

The signature of useful entanglement for sub–shot-noise interferometry is a Fisher information larger than the total number of particles $\mathcal{F} > N_{tot}$ (*6*). The Fisher information also provides the ultimate achievable sensitivity via the Cramer-Rao bound $\Delta\theta \geq 1/\sqrt{n\mathcal{F}}$, which can be reached asymptotically for a large number of measurements *n*. However, here, as well as in previous experiments on squeezing, entanglement, and quantum interferometry with ultracold atoms, the total number of particles fluctuates in different realizations; thus, the entanglement criteria must be generalized by replacing the fixed number of particles N_{tot} with its statistical average $\langle N_{tot} \rangle$ (*32*). A lower bound for the Fisher information is provided by $\mathcal{F} \geq |d\langle J_z^2 \rangle / d\theta|^2 / (\Delta J_z^2)^2$. In our experiment, this lower bound is maximized for an angle of 0.015 rad, resulting from the finite detection efficiency. At this angle, we obtain $\mathcal{F}/\langle N_{tot} \rangle \geq 1.45^{+042}_{-0.29}$, where a value greater than 1 proves entanglement. This entanglement can be exploited for sub–shot-noise phase estimation in a large variety of interferometer configurations (*33*), including the Ramsey interferometer.

The presented results are mainly restricted by the detection limit of 20 atoms. A detection limit of 5 atoms would allow for a minimum phase estimation uncertainty of −13.6 dB below the shot noise limit (*29*). Furthermore, the region of sub–shot-noise interferometry can be extended up to the whole phase domain by using maximum likelihood or Bayesian phase estimation protocols. The combination of large samples and quantum-enhanced sensitivity should open exciting

perspectives for highly sensitive measurements with a new generation of atom interferometers.

Bücker *et al*. (*34*) recently reported reduced atom number fluctuations in twin-atom beams, and the group of M. Oberthaler has independently used spin dynamics in Bose-Einstein condensates to generate atomic two-mode entanglement detected by a homodyning technique.

References and Notes

1. N. F. Ramsey, *Phys. Rev.* **78**, 695 (1950).
2. C. Bordé, *Phys. Lett. A* **140**, 10 (1989).
3. L. Essen, J. V. L. Parry, *Nature* **176**, 280 (1955).
4. R. Wynands, S. Weyers, *Metrologia* **42**, S64 (2005).
5. G. Santarelli *et al*., *Phys. Rev. Lett.* **82**, 4619 (1999).
6. L. Pezzé, A. Smerzi, *Phys. Rev. Lett.* **102**, 100401 (2009).
7. J. Appel *et al*., *Proc. Natl. Acad. Sci. U.S.A.* **106**, 10960 (2009).
8. J. Estève, C. Gross, A. Weller, S. Giovanazzi, M. K. Oberthaler, *Nature* **455**, 1216 (2008).
9. C. Gross, T. Zibold, E. Nicklas, J. Estève, M. K. Oberthaler, *Nature* **464**, 1165 (2010).
10. I. D. Leroux, M. H. Schleier-Smith, V. Vuletić, *Phys. Rev. Lett.* **104**, 073602 (2010).
11. M. F. Riedel *et al*., *Nature* **464**, 1170 (2010).
12. Z. Chen, J. G. Bohnet, S. R. Sankar, J. Dai, J. K. Thompson, *Phys. Rev. Lett.* **106**, 133601 (2011).
13. J. J. Bollinger, W. M. Itano, D. J. Wineland, D. J. Heinzen, *Phys. Rev. A* **54**, R4649 (1996).
14. M. J. Holland, K. Burnett, *Phys. Rev. Lett.* **71**, 1355 (1993).
15. A. Kuzmich, L. Mandel, *Quantum Semiclass. Opt.* **10**, 493 (1998).
16. Z. Y. Ou, J.-K. Rhee, L. J. Wang, *Phys. Rev. Lett.* **83**, 959 (1999).
17. P. Walther *et al*., *Nature* **429**, 158 (2004).
18. M. W. Mitchell, J. S. Lundeen, A. M. Steinberg, *Nature* **429**, 161 (2004).
19. I. Afek, O. Ambar, Y. Silberberg, *Science* **328**, 879 (2010).
20. V. Meyer *et al*., *Phys. Rev. Lett.* **86**, 5870 (2001).
21. D. Leibfried *et al*., *Nature* **438**, 639 (2005).
22. L.-M. Duan, A. Sørensen, J. I. Cirac, P. Zoller, *Phys. Rev. Lett.* **85**, 3991 (2000).
23. H. Pu, P. Meystre, *Phys. Rev. Lett.* **85**, 3987 (2000).
24. T. Kim, O. Pfister, M. J. Holland, J. Noh, J. L. Hall, *Phys. Rev. A* **57**, 4004 (1998).
25. T. Nagata, R. Okamoto, J. L. O'brien, K. Sasaki, S. Takeuchi, *Science* **316**, 726 (2007).
26. C. Klempt *et al*., *Phys. Rev. Lett.* **104**, 195303 (2010).
27. S. M. Barnett, D. T. Pegg, *Phys. Rev. A* **42**, 6713 (1990).
28. M. Scherer *et al*., *Phys. Rev. Lett.* **105**, 135302 (2010).
29. Supporting material is available on *Science* Online.
30. C. Klempt *et al*., *Phys. Rev. Lett.* **103**, 195302 (2009).
31. R. A. Campos, B. E. A. Saleh, M. C. Teich, *Phys. Rev. A* **40**, 1371 (1989).
32. P. Hyllus, L. Pezzé, A. Smerzi, *Phys. Rev. Lett.* **105**, 120501 (2010).
33. P. Hyllus, O. Gühne, A. Smerzi, *Phys. Rev. A* **82**, 012337 (2010).
34. R. Bücker *et al*., *Nat. Phys.* **7**, 608 (2011).

Acknowledgments: We thank E. Rasel for stimulating discussions and P. Zoller for helpful comments. We acknowledge support from the Centre for Quantum Engineering and Space-Time Research (QUEST), the European Science Foundation (EuroQUASAR), and the Danish National Research Foundation Center for Quantum Optics. P.H. acknowledges financial support of the European Research Council Starting Grant GEDENTQOPT. This work was supported in part by Provincia Autonoma di Trento within the activities of the BEC center. L.P. acknowledges support by the Laboratoire Charles Fabry de L'Institut d' Optique where part of this work was completed.

Supporting Online Material

www.sciencemag.org/cgi/content/full/science.1208798/DC1
SOM Text
Figs. S1 to S5
References (*35*–*40*)

23 May 2011; accepted 23 September 2011
Published online 13 October 2011;
10.1126/science.1208798

Direct Observation of Molecular Preorganization for Chirality Transfer on a Catalyst Surface

Vincent Demers-Carpentier,[1] Guillaume Goubert,[1] Federico Masini,[1] Raphael Lafleur-Lambert,[1] Yi Dong,[1] Stéphane Lavoie,[1] Gautier Mahieu,[1] John Boukouvalas,[1] Haili Gao,[2] Anton M. H. Rasmussen,[2] Lara Ferrighi,[2] Yunxiang Pan,[2] Bjørk Hammer,[2]* Peter H. McBreen[1]*

The chemisorption of specific optically active compounds on metal surfaces can create catalytically active chirality transfer sites. However, the mechanism through which these sites bias the stereoselectivity of reactions (typically hydrogenations) is generally assumed to be so complex that continued progress in the area is uncertain. We show that the investigation of heterogeneous asymmetric induction with single-site resolution sufficient to distinguish stereochemical conformations at the submolecular level is finally accessible. A combination of scanning tunneling microscopy and density functional theory calculations reveals the stereodirecting forces governing preorganization into precise chiral modifier-substrate bimolecular surface complexes. The study shows that the chiral modifier induces prochiral switching on the surface and that different prochiral ratios prevail at different submolecular binding sites on the modifier at the reaction temperature.

Chirality transfer and amplification on surfaces is fundamentally important to progress in the synthesis of enantiopure compounds for pharmaceutical and agrochemical applications (*1*–*4*) and to discussions of the origin of biological homochirality (*5*). Chirally modified heterogeneous catalysts, in which the reaction is stereocontrolled at surface sites formed by adsorbing a chiral molecule, offer a number of sought-after advantages, including ease of separation of the catalyst from the product. The best-explored examples in terms of potential applications involve the hydrogenation of activated ketones to chiral alcohols and hydroxy esters on cinchona-modified Pt (*6*, *7*). A number of synthetic modifiers that share some key structural and functional characteristics of cinchonidine, such as 1-(1-naphthyl)ethylamine (NEA) and its condensation derivatives (*8*), can also be used. However, a lack of mechanistic understanding has long been seen as an impediment to the rational development of chirally modified heterogeneous catalysts (*6*, *7*).

We directly characterized the surface complexation of a prochiral reagent with a chiral modifier by using 2,2,2-trifluoroacetophenone, TFAP, as the prochiral substrate, (*R*)-(+)-NEA as the modifier, and Pt(111) as the metal surface. Preorganization in this chemisorption system can be described in terms of molecular recognition between a fully chiral molecule and a molecule that is chiral only by virtue of its confinement on the surface (*4*, *9*–*15*). The experiment resolves interactions at the level of functional groups at individual modifier sites and thereby provides insight into the structural preorganization that biases the stereochemical outcome of the reaction, in essence the mechanism of chirality transfer. The scanning tunneling microscopy (STM) measurements were carried out at room temperature in parallel with room temperature catalytic measurements on the asymmetric hydrogenation of TFAP to 2,2,2-trifluorophenylethanol over (*R*)-NEA modified Pt on an alumina support.

The interactions of the chiral modifier and the prochiral substrate with the metal surface were first studied separately. Two modifier motifs, present in a 7:3 ratio, are observed in the STM images (Fig. 1, A and B). The two motifs may be distinguished by the position of the bright protrusion: It extends from the central region of the image in the majority motif (A) and from the left-hand side in the minority motif (B). The two lowest energy structures predicted by density functional theory (DFT) are the (*R*)-NEA-1 and (*R*)-NEA-2 conformers (Fig. 1, E and F). Their calculated adsorption energies are ~2 eV with a pronounced 0.13 eV preference for the (*R*)-NEA-1 conformation (figs. S10 and S11), suggesting that their relative surface coverages are determined in part by adsorption dynamics. Surface vibrational spectroscopy measurements (figs. S1 and S2) confirm that the NEA conformers are chemisorbed in the geometry found in the DFT calculations. In particular, the C-CH_3 bond is nearly perpendicular to the surface, as also described for the Pd(111) surface (*16*).

[1]Centre de recherche sur les propriétés des interfaces et la catalyse (CERPIC) and Département de chimie, Université Laval, Québec, QC G1V 0A6, Canada. [2]Interdisciplinary Nanoscience Center (iNANO) and Department of Physics and Astronomy, Aarhus University, DK 8000 Aarhus, Denmark.

*To whom correspondence should be addressed. E-mail: hammer@phys.au.dk (B.H.); peter.mcbreen@chm.ulaval.ca (P.H.M.)